Generalized sixth-order dispersion solitons

Y. Long Qiang,[1,*] Tristram J. Alexander,[1] and C. Martijn de Sterke[1,2]
[1]*Institute of Photonics and Optical Science (IPOS), School of Physics, The University of Sydney, NSW 2006, Australia*
[2]*The University of Sydney Nano Institute (Sydney Nano), The University of Sydney, NSW 2006, Australia*

(Received 8 September 2021; accepted 6 January 2022; published 2 February 2022)

Encouraged by recent experimental breakthroughs, we investigate the types of bright solitons that can exist in the presence of a Kerr nonlinearity and quadratic, quartic, and sextic dispersion by examining the nature of the soliton tails. We verify the soliton shape by full numerical calculations and find analytic solutions for some parameters. We reveal the sensitivity of the interaction dynamics to the particular choice of the dispersion parameters. These results provide a framework for experiments in this regime and for exploring parameter spaces with even higher dimensions.

DOI: 10.1103/PhysRevA.105.023501

I. INTRODUCTION

Conventional optical solitons, pulses that retain their shape through the balance of the Kerr nonlinearity and quadratic dispersion, have been extensively studied [1–5]. Solitons have numerous optical applications, including in ultrafast lasers [6,7], telecommunication systems [8–11], and supercontinuum generation [12–14]. Since quadratic dispersion is generically the dispersion of lowest order, higher orders of dispersion have traditionally been considered to be a perturbation. Examples are the work of Karlsson and Höök [15] and Akhmediev *et al.*, who investigated solitons in the presence of both quadratic and quartic dispersion [16]. Karlsson and Höök found a stable analytic solution [15], which was confirmed by Piché *et al.* [17], whereas Akhmediev *et al.*, working in a different parameter regime, reported different stable solitons with oscillations in the tails. The effects of cubic dispersion has also been investigated [18–22], but here we focus on even orders.

The recent discovery of pure quartic solitons, entirely dependent on negative quartic dispersion, rather than quadratic dispersion, has changed our perception of optical solitons, and has opened up new areas to explore [23–25]. Pure quartic solitons were discovered in a silicon photonic crystal waveguide in which the quadratic and cubic dispersion are negligible at a particular wavelength and the quartic dispersion is negative [25]. This work was followed by a thorough theoretical investigation of these solitons [23]. Runge *et al.* subsequently reported a fiber laser that contains an adjustable pulse shaper and that can emit solitons with programmable dispersion [26]. This not only enabled a complete study of pure-quartic solitons, but also opened the way to the investigation of solitons with other unusual types of dispersion. For example, this laser was used to demonstrate the experimental observation of pure higher order solitons with dispersion up to 10^{th} order, which was accompanied by numerical results up to the 16^{th} order [27].

The laser of Runge *et al.* is not only able to emit solitons with pure orders of dispersion, but also with mixed orders of dispersion [28]. It is therefore important to consider how the interplay of different dispersion orders affects the soliton characteristics. The parameter space of pulselike solutions with quadratic and negative quartic dispersion was investigated analytically and numerically by Tam *et al.* [24]. This work revealed a large family of soliton solutions with varying pulse shapes of which the analytic solution of Karlsson and Höök [15], and the solutions with oscillating tails of Akhmediev *et al.* [16] are natural members, putting them in a wider conceptual framework. This work analytically divided the parameter space into regions with exponential tails, oscillating tails, and a region that does not support pulselike solutions [24].

Having acquired an understanding of the three-dimensional parameter space spanned by the nonlinearly induced phase shift, and the quadratic (second order) and quartic (fourth order) dispersion, it is natural to consider even higher dispersion orders. Therefore, in this paper we investigate the four-dimensional parameter space that also includes negative sextic (sixth order) dispersion. We introduce novel solution regions, distinct from the results with second-order and fourth-order dispersion and help to outline approaches for analyzing bright pulselike soliton solutions at any dispersion order.

The first step in our investigations is an analysis of the tails of the solutions, where the nonlinear effect can be neglected. The parameter space we are considering can have solitons with exponentially decaying tails and solitons with oscillatory tails, but these behaviors compete, requiring us to identify the dominant effect. The competition is stronger and more varied in our four-dimensional parameter space, compared to the three-dimensional parameter space considered before [24]. We find boundaries demarcating the different behaviors, one of which is new and has no equivalent in the fourth-order dispersion case [24].

Since the interaction between solitons is mediated by their tails [29,30], it is interesting to consider how the oscillations affect the mutual interaction. To this end we conduct studies of the dynamics of coupled pulses within different regions of

*yqia7452@uni.sydney.edu.au

parameter space, qualitatively observing the interaction. We find that solutions from regions with oscillating tails can repel or attract depending on the initial separation. In contrast, for solitons with exponential tails the interaction always has the same sign.

As part of our studies of the large parameter space we also find an exact analytic solution, analogous to that of Karlsson and Höök for the pure quartic case [15]. Our results are numerically confirmed, and promise an avenue into finding more families of exact analytic solutions within the expanded parameter space. Numerical evolution studies imply that all of these solutions are stable.

The outline of this paper is as follows. In Sec. II we outline our mathematical model. In Sec. III we investigate the possible pulselike solutions in the parameter space of the nonlinear phase shift, and the second-order, fourth-order, and (negative) sixth-order dispersion coefficients. However, we first consider a special case in Sec. III A, with additional ones discussed in Secs. A 1 and A 2. Whereas the work in Sec. III is analytic, in Sec. IV we augment this with fully numerical static soliton solutions and with extension of the Karlsson and Höök solution [15] to 6$^{\text{th}}$ order dispersion. In Sec. V we present our investigation of the interaction dynamics. In Sec. VI we discuss our results and conclude.

II. MODEL

We consider the possible solutions for optical solitons when combining the effects of even order dispersion effects up to sixth-order dispersion. The evolution of these solitons can be described by the modified nonlinear Schrödinger equation:

$$i\frac{\partial\psi}{\partial z}-\frac{\beta_2}{2}\frac{\partial^2\psi}{\partial T^2}+\frac{\beta_4}{24}\frac{\partial^4\psi}{\partial T^4}-\frac{\beta_6}{720}\frac{\partial^6\psi}{\partial T^6}+\gamma|\psi|^2\psi=0, \quad (1)$$

where $\psi(z,T)$ is the pulse envelope, z the propagation coordinate, T the local time, and γ the nonlinear parameter, which we take to be positive. The β_n are the n^{th}-order dispersion coefficients, where $\beta_n \equiv \partial^n\beta/\partial\omega^n = \partial^{n-1}v_g^{-1}/\partial\omega^{n-1}$, with β the mode propagation constant and v_g the group velocity.

We are interested in stationary solutions of the form $\psi(z,T)=u(T;\mu)e^{i\mu z}$, which satisfy

$$-\mu u-\frac{\beta_2}{2}\frac{d^2u}{dT^2}+\frac{\beta_4}{24}\frac{d^4u}{dT^4}+\frac{|\beta_6|}{720}\frac{d^6u}{dT^6}+\gamma u^3=0, \quad (2)$$

and where u can be taken to be real. We have taken $\beta_6<0$ as is necessary for the existence of bright, pulselike solutions. For the existence of such solutions it is moreover necessary that $\mu>0$; if $\mu<0$, the soliton spectrum intersects the linear dispersion relation leading to energy exchange between the soliton and linear waves, so the soliton cannot be stationary.

We can find necessary conditions for soliton existence, and gain insight into the soliton properties, by examining the linear wave solutions to Eq. (2), under the linear approximation ($\gamma=0$), valid when the wave amplitude is small. The solutions to the resulting equation are linear combinations of terms of the form $\exp(\lambda\tau)$. The λ satisfy the algebraic equation,

$$-\mu-\frac{\beta_2}{2}\lambda^2+\frac{\beta_4}{24}\lambda^4+\frac{|\beta_6|}{720}\lambda^6=0. \quad (3)$$

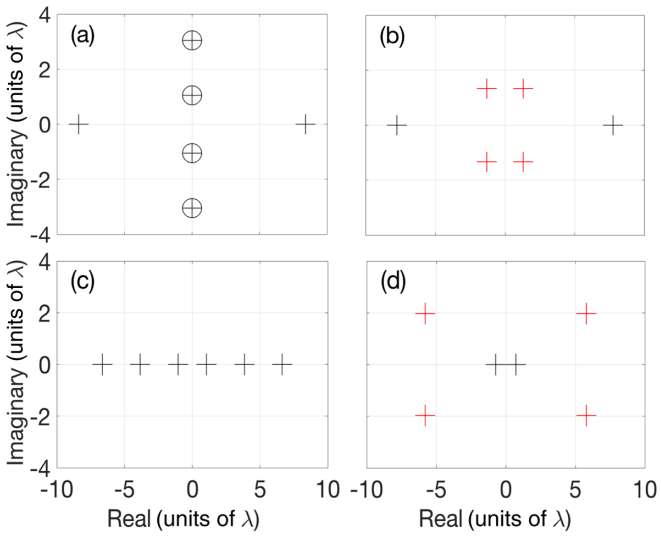

FIG. 1. Schematic of the four root configurations of Eq. (3), indicating the nature of the tail of the soliton solutions. Here $\beta_6=-1$ ps^{6}mm^{-1}, $\beta_4=-2$ ps^{4}mm^{-1}, and $\mu=1$ mm^{-1}. (a) $\beta_2=2$ ps^{2}mm^{-1} (Configuration A); (b) $\beta_2=0$ ps^{2}mm^{-1} (Configuration B); (c) $\beta_2=-2$ ps^{2}mm^{-1} (Configuration C); and (d) $\beta_2=-4$ ps^{2}mm^{-1} (Configuration D). Each is indicated by green dots in Fig. 3(a). Features of the configurations are summarized in Table I.

In Sec. III we identify the possible linear wave solutions to Eq. (3), and infer from these solutions the nature of possible associated soliton solutions. In Sec. IV we validate our linear analysis with numerically and analytically calculated soliton solutions to Eq. (2) and confirm their existence.

III. LINEAR ANALYSIS

In order to identify the properties of soliton solutions in the sixth-order dispersion case, we employ linear analysis on Eq. (3), noting first that it has six roots. The positions of these roots in the complex plane allow us to draw analytic conclusions regarding the tails of the soliton solutions [16,23,27]. Since Eq. (3) is a cubic equation in λ^2 with real coefficients, the possible combinations of the roots is limited. The solutions consist of pairs of real solutions ($\pm\lambda$), pairs of imaginary solutions (λ, $\lambda^\star$) or, equivalently ($\pm\lambda$), or a quartet of complex solutions ($\pm\lambda$, $\pm\lambda^\star$). Since the existence of bright, pulselike solutions requires $\mu>0$, the product of all six roots needs to be positive. This implies that the only allowed configurations of the roots are (i) two pairs of imaginary roots and one pair of real roots [Configuration A; see Fig. 1(a)]; (ii) a quartet of complex roots and a pair of real roots [Configurations B and D; see Figs. 1(b) and 1(d)]; and (iii) three pairs of real roots [Configuration C; Fig. 1(c)].

Imaginary roots, as in Configuration A [Fig. 1(a)], correspond to harmonically varying solutions that do not decay; hence such roots preclude pulselike solutions (unless the associated coefficients vanish). In the coming sections Configuration A is indicated with a black color on the parameter plane. In contrast, real roots correspond to exponentially decaying solutions as $T\to\pm\infty$ whereas complex roots correspond to oscillating tails [16]. For every root λ, the sign of the real part determines the direction of decay. For $\text{Re}(\lambda)>0$,

TABLE I. Overview of the four distinct root configurations, illustrated in Fig. 1, and their features. The "color" entries refer to the color coding of the regions in Figs. 2 and 3.

Label	Root composition	Tail	Color	Localized solution
A	4 Imaginary, 2 Real	Trigonometric	Black	No
B	2 Real, 4 Complex	Exponential, oscillatory	Dark gray	Yes
C	6 Real	Exponential	White	Yes
D	2 Real, 4 Complex	Exponential	Light gray	Yes

the corresponding roots describe the trailing edge of the pulse and for $\mathrm{Re}(\lambda) < 0$, the roots describe the leading edge.

The root Configurations B, C, and D [Figs 1(b), 1(c), and 1(d)] correspond to pulselike, localized solutions. Since the tails are a sum of exponentials, we expect the roots that decay most slowly to dominate [27], i.e., the roots for which $|\mathrm{Re}[\lambda]|$ is smallest. Thus in Configuration B [Fig. 1(b)], in which the complex roots dominate, the solutions have oscillating tails [16,23,25,27]. Such solutions are indicated by the dark gray color on the parameter plane. In Configuration C [Fig. 1(c)] the tails decay exponentially; while in Configuration D [Fig. 1(d)] the real roots dominate and the tails also decay exponentially. These solutions are represented in white and light gray, respectively, on the parameter plane. The labels and properties of these four regions are summarized in Table I. We note that configurations B and D, which combine real roots and a quartet of complex roots require at least sixth-order dispersion, and hence were absent in previous studies [24].

We use these distinct regions to define the parameter space spanned by the parameters β_6, β_4, β_2, and μ in Eq. (2). This equation shows that there are only three free parameters, since we can divide through by β_6, or, alternatively, fix β_6. Based on the configuration of the roots we can then predict the type of solution. Note that when $\mu \to \infty$, the sixth-order dispersion dominates and the roots form a perfect hexagon, which is a special case of Configuration B. We first consider the special case, when $\beta_4 = 0$, before considering the general case. We consider two additional special cases in Appendices A 1 and A 2.

A. Special case: $\beta_2 \neq 0$ and $\beta_4 = 0$

When $\beta_4 = 0$, tail Eq. (3) simplifies to

$$-\mu - \frac{\beta_2}{2}\lambda^2 + \frac{|\beta_6|}{720}(\lambda^2)^3 = 0, \tag{4}$$

which is a cubic polynomial in λ^2. For $\beta_2 > 0$, this polynomial has one positive real root, and either two complex roots or two negative real roots. Negative real roots of λ^2 correspond to imaginary roots for λ, and consequently solutions with no localized pulse (Region A). Alternatively, a pair of complex conjugate roots of λ^2 correspond to a quartet of complex roots for λ, and when these roots dominate [as in Fig. 1(b)] the tails decay with oscillations (Region B). The boundary between these regions is given by

$$\mu_0 = \frac{\beta_2}{3}\sqrt{\frac{120\beta_2}{|\beta_6|}}, \tag{5}$$

illustrated in Fig. 2, separating Regions A and B.

For $\beta_2 < 0$, λ^2 has a positive real root and a complex conjugate pair of roots with negative real part. In terms of λ, therefore, there are always two real roots and a quartet of complex roots. The only remaining issue is whether the configuration is B or D [Fig. 1(b) or 1(d)]. To determine this we find the boundary μ_c between these regions, by considering a sextic polynomial with real roots $\pm a_r$ and complex roots $\pm a_r \pm i a_i$. The condition for the coefficient of λ^4 to vanish is $a_i^2 = 3a_r^2/2$, which corresponds to setting $\beta_4 = 0$ in the polynomial. Using this result and by matching with Eq. (4), it is then straightforward to derive the boundary,

$$\mu_c = \frac{50}{147}\sqrt{-210\frac{\beta_2^3}{|\beta_6|}}, \tag{6}$$

separating solutions with dominant real roots (Region D), from those with dominant complex roots (Region B). The complete parameter plane for $\beta_4 = 0$ is in Fig. 2.

The boundary μ_c requires a quartet of complex roots as well as a pair of real roots, all with real parts of the same magnitude. This requires the presence of at least six roots, and hence dispersion of at least sixth order. In contrast, in the fourth-order case, there only are boundaries of type such as μ_0 [see Eq. (5)], which mark the transition between roots on the real or imaginary axis, and roots in the complex plane [24].

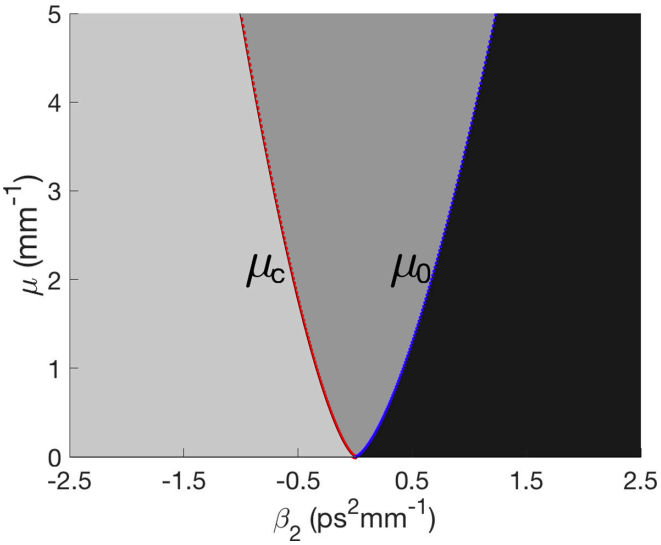

FIG. 2. Cross section through parameter space for $\beta_4 = 0$ and $\beta_6 = -1\ \mathrm{ps}^6\ \mathrm{mm}^{-1}$. The colors correspond to root configurations given in Table I. The boundaries μ_0 and μ_c are given in Eq. (5) and (6), respectively.

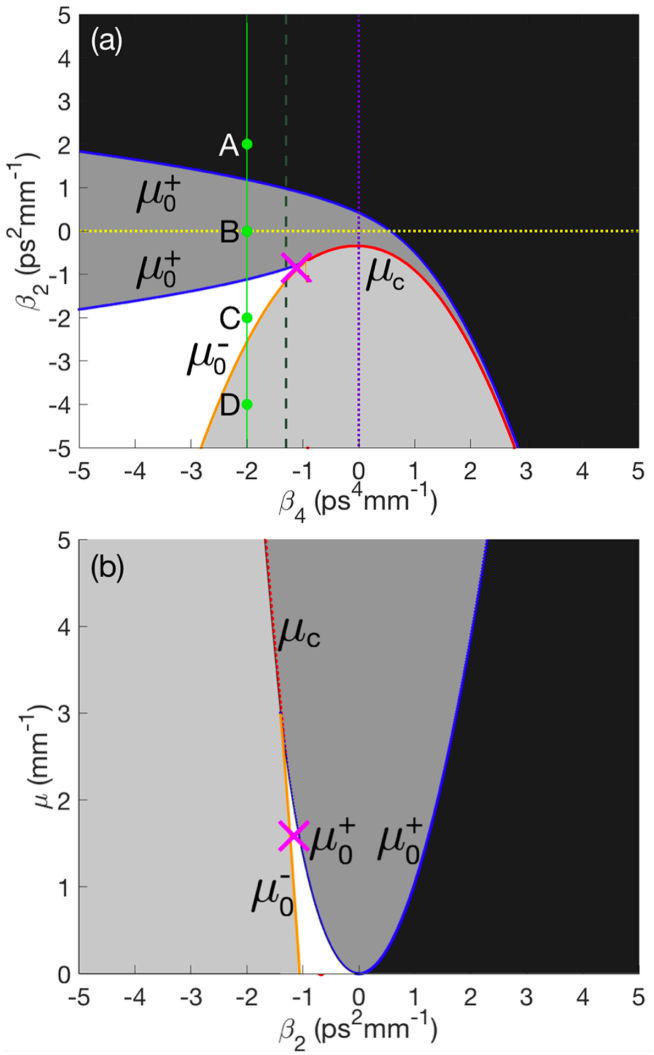

FIG. 3. Cross sections taken through the general parameter space with $\beta_6 = -1$ ps^6 mm^{-1}. (a) $\mu = 1$ mm^{-1}; (b) $\beta_4 = -1.3$ ps^4 mm^{-1}. The colors correspond to the regions given in Table I. (Yellow dotted line) $\beta_2 = 0$; (purple dotted line) $\beta_4 = 0$; (dark blue and orange curves) $\mu_0^{\pm}$ [Eq. (7)]; (red curve) μ_c [Eq. (8)]; (dark green dotted line) cross section of $\beta_4 = -1.3$ ps^4 mm^{-1} in (a) corresponding to (b); (pink crosses) hyperbolic secant exact solution discussed in Sec. IV B; (light green line) A, B, C, and D correspond to the root configurations in Fig. 1.

B. General case

We now consider the general case with arbitrary $\beta_{2,4}$ and μ. In contrast to Sec. III A, our parameter space is now four-dimensional. In order to visualize the general case, we fix β_6 and use two two-dimensional cross sections of the resulting three-dimensional parameter space. These cross sections [see Figs. 3(a) and 3(b)] exhibit all four of the regions, including Region C, indicated in white, in which all roots are real. Though this configuration does not occur in Sec. III A, it does arise in the special case when μ is small (see Appendix A 2).

We can obtain the boundaries for these generalized regions analytically, by considering the cubic discriminant Δ [31] of Eq. (3) in terms of λ^2. For a cubic discriminant Δ, the condition $\Delta = 0$ corresponds to the boundary between three cubic real roots ($\Delta > 0$) and one cubic real root and two cubic complex roots ($\Delta < 0$). For Eq. (3) this corresponds to the boundary between Configurations B and D, and Configurations A and C. We obtain the analytic boundaries $\mu_0^{\pm}$ separating these regions by rearranging the condition $\Delta = 0$, leading to

$$\mu_0^{\pm} = \frac{25\beta_4^3 + 45\beta_2\beta_4|\beta_6| \pm \sqrt{5}\sqrt{\left(5\beta_4^2 + 6\beta_2|\beta_6|\right)^3}}{9|\beta_6|^2}. \quad (7)$$

The boundaries $\mu_0^{\pm}$ indicate when the cubic discriminant changes sign, and as seen in Fig. 3, separate Regions A and B, B and C, and C and D. We note that Region C, with six real roots, requires $\beta_{2,4} < 0$, which explains why this region was not present in the special cases in Secs. III A and A 1. In the general case, it is bounded by both boundaries $\mu_0^{\pm}$. The boundary μ_0^+, which separates Regions B and C, is analogous to the boundary in the fourth-order dispersion case between pulselike solutions with exponential and oscillatory tails [24].

The final key boundary to be analytically identified is the boundary μ_c, separating Regions B and D. Following the same procedure as in Sec. III A, we determine the boundary to be given by

$$\mu_c = \frac{|\beta_6|}{720}w^3 + w^2 s + wt, \quad (8)$$

where $s = 30\beta_4/|\beta_6|$, $t = -30\beta_2/|\beta_6|$, $r = -720\mu/|\beta_6|$, and $w = (-6s \pm \sqrt{-48s^2 + 336t})/42$. This boundary is similar to that given by Eq. (5) in Sec. III A.

We now have obtained an analytic expression for all the boundaries between each of the regions for Eq. (3) in the general case. As illustrated in Fig. 3, we have developed the analytic framework to categorize all pulselike stationary solutions of Eq. (1) in terms of the four distinct regions defined by our root tail analysis. The purple dotted line represents the special case $\beta_4 = 0$ from Sec. III A and is consistent with Fig. 2. The yellow dotted line represents the special case $\beta_2 = 0$ discussed in Appendix A 1 and is consistent with Fig. 7.

IV. SOLITON SOLUTIONS

A. Numerical solutions

We can solve Eq. (2) numerically using the Newton conjugate-gradient method [26,32], giving solutions in any region with decaying tails. In this way we confirm the allocation of parameter space outlined in Sec. III, and the existence of the single peak pulselike solutions.

Figures 4(a) and 4(b) show a single peak solution on linear and logarithmic scales, respectively, with a root structure from Region C. However, the solutions are also representative of solutions found in Region D. For both regions, the real roots dominate and the tails are exponentially decreasing. Figures 4(c) and 4(d) show a solution from Region B. The tail oscillations are consistent with our analysis. Both of these solutions are similar to those found in the presence of mixed second- and fourth-order dispersion [24].

In contrast, the solution shown in Figs. 4(e) and 4(f), close to the μ_c boundary, is novel and requires sixth-order dispersion. Note the low-amplitude oscillations, reflecting that

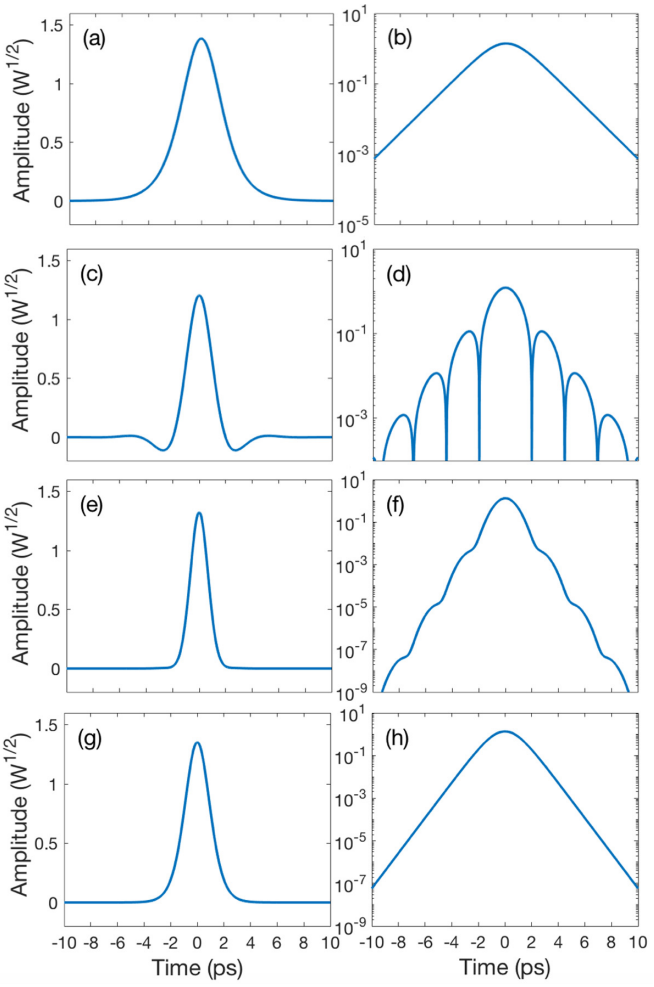

FIG. 4. Soliton amplitude versus time for $\beta_6 = -1$ ps^{6}mm^{-1}, $\gamma = 1\ W^{-1}$ mm^{-1} and $\mu = 1$ mm^{-1} for (a) solution with exponential tails with $\beta_2 = -3$ ps^{2}mm^{-1}, $\beta_4 = -4$ ps^{4}mm^{-1} on a linear scale, and (b) on a logarithmic scale. (c) and (d) Same as (a) and (b) but for a solution with oscillatory tails with $\beta_2 = 0.5$ ps^{2}mm^{-1}, $\beta_4 = -4$ ps^{4}mm^{-1}. (e) and (f) Solution close to boundary μ_c with $\beta_2 = -0.34$ ps^{2}mm^{-1}, $\beta_4 = -0.1$ ps^{4}mm^{-1}. (g) and (h) Exact analytic solution (purple crosses in Fig. 3) with $\beta_2 = -0.8518$ ps^{2}mm^{-1}, $\beta_4 = -1.11415$ ps^{4}mm^{-1}.

the exponentially decaying tails and the oscillating tails are approximately equally strong. These features are observed in both regions close to μ_c, and confirm the analytic features we predicted in Sec. III A.

B. Exact analytic solution

The traditional soliton with second-order dispersion is an exact analytic solution to the nonlinear Schrödinger equation [33,34]. For higher order dispersion, however, analytic solutions have been far more difficult to find. Karlsson and Höök's solution in the form of the square of a hyperbolic secant for mixed second-order and fourth-order dispersion is amongst the few that have been reported [35]. Here, we expand upon this solution to obtain an analytic solution of Eq. (2).

For the mixed sixth-order case, we assume an exact analytic solution of the form,

$$u = A\ \mathrm{sech}^3(\alpha\tau), \tag{9}$$

where A and α are as yet unknown constants and find the associated parameters in Eq. (2). To do so, we note that the second derivative of the power of a hyperbolic secant function satisfies

$$\frac{d^2\mathrm{sech}^p(\tau)}{d\tau^2} = p^2\mathrm{sech}^p(\tau) - p(p+1)\mathrm{sech}^{p+2}(\tau). \tag{10}$$

Using this when substituting Eq. (9) into Eq. (2) we find

$$-\mu A\mathrm{sech}^3(\alpha\tau) + \sum_{q=3}^{9} A_q \mathrm{sech}^q(\alpha\tau) + \gamma(A\mathrm{sech}^3(\alpha\tau))^3 = 0, \tag{11}$$

where the A_q are constants that can be found from Eq. (10) and the summation only involves odd powers.

The linear terms in Eq. (11) consist of hyperbolic secant terms of order 3, 5, 7, and 9 whereas the nonlinear term is of order 9. For the equation to be satisfied, the prefactors for each order of hyperbolic secant must cancel. Thus the nonlinear term, which is ninth order, must match the ninth order originating from the sixth-order derivative. This gives

$$\gamma \mathrm{A}^2 = \frac{8!}{6!\ 2}|\beta_6|\alpha^6 = 28|\beta_6|\alpha^6. \tag{12}$$

Repeating this process for the lower orders 3, 5, and 7, all of which originate from the linear terms, we obtain expressions for the unknown coefficients,

$$\alpha^2 = -\frac{30}{83}\frac{\beta_4}{|\beta_6|}, \quad \beta_2 = \frac{1891|\beta_6|}{360}\alpha^4, \quad \mu = \frac{245|\beta_6|}{16}\alpha^6. \tag{13}$$

Figures 4(g) and 4(h) show this solution, which is consistent with the numerical result based on the Newton conjugate-gradient method [32]. The location of this solution in parameter space is shown by the purple cross in Fig. 3, and is always located in Region C. Karlsson and Höök's solution in the fourth-order dispersion case is analogous in that it has solutions that are exclusively located in the region with only real roots, and thus both have exponential tails.

Equations (12) and (13) show that we can choose β_4 β_6, and γ freely, and all other parameters are then given. Thus, solitons as in Eq. (9) only exist in media with particular dispersion relations, and they have a particular amplitude: Given β_4 and β_6, then β_2 is prescribed, and, given γ, so are A and μ. This contrasts with conventional nonlinear Schrödinger solitons which exist for any β_2 and any amplitude [5], and for the solutions of Karlsson and Höök [15] for which β_2 and β_4 can be chosen freely, but not the amplitude. These differences can be understood as follows: The solutions have three degrees of freedom (A, α, and μ), whereas the number of constraints is given by the number of orders that enter equations of the type Eq. (11). For conventional solitons $q = 1, 3$, so there are two constraints, leaving one degree of freedom. For the solutions of Karlsson and Höök $q = 2, 4, 6$, so there is no freedom left. For solution (9) $q = 3, 5, 7, 9$ and so there is one more constraint than degrees of freedom and so one of the dispersion coefficients is prescribed.

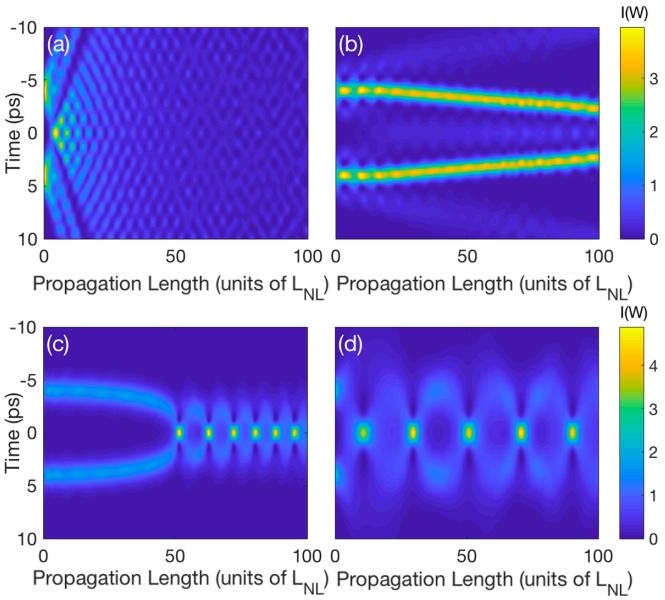

FIG. 5. Propagation of Gaussian pulses separated by 8 ps for parameters shown by the green dots in Fig. 3(a), corresponding to Configurations (a) A, (b) B, (c) C, and (d) D. The dispersion parameters are given for the corresponding configurations in Fig. 1.

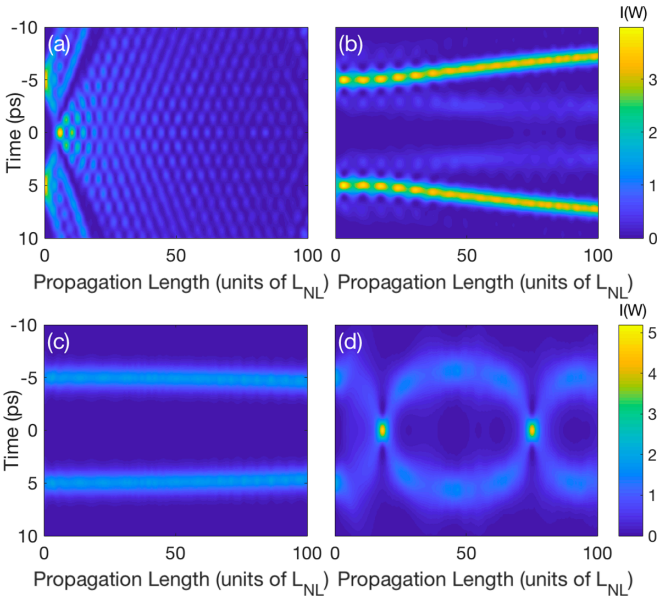

FIG. 6. As Fig. 5, but with the Gaussian pulses separated by 10 ps.

V. DYNAMIC RESULTS

In this section we determine numerically the stability of our soliton solutions, and qualitatively investigate the role of the soliton tails in the soliton interaction dynamics. We solve the model Eq. (1) numerically using a split-step Fourier method [32]. All simulations are carried out over a propagation distance of $100L_{\mathrm{NL}}$, where

$$L_{\mathrm{NL}} = 1/(\gamma P), \tag{14}$$

and P is the pulse's peak power [5]. We take the nonlinear length since the dispersion length is not uniquely defined in the presence of mixed dispersion. Since the solutions we are investigating balance the effects of the dispersion and the nonlinearity, we use L_{NL} as a proxy for the combined effects of all dispersion orders. In all cases we found that the stationary solutions appear to be stable. We do not show results of these studies, but rather consider the dynamics of coupled solitons for each region in the parameter plane as they interact through their low-amplitude tails. Solving Eq. (1) numerically through the split-step Fourier method, allows us to examine the dynamics of these interacting pulses.

We take two identical, in-phase Gaussian pulses, separated in time as the initial condition. All have the full width at half-maximum of 2.44 ps and peak intensity of 1.94 W, roughly corresponding to the full solutions indicated by the green dots for Configurations C and D in Fig. 3(a). By keeping a constant Gaussian initial condition as the input pulse, we eliminate the possible effect of the input pulse on the interaction dynamics, allowing us to concentrate exclusively on the effects of the dispersion. The initial separations are taken to be 8 ps (Fig. 5) and 10 ps (Fig. 6), ensuring that the pulses interact weakly. Taking all input pulses to be identical allows us to observe the dependence of the interaction on the properties of the soliton tails for Configurations A–D, and removing the dependence on the detailed properties of the input pulses.

Figures 5(a) and 6(a) both correspond to Configuration A where no pulselike solutions can exist. This initial condition almost immediately transforms into a purely oscillatory solution, as expected. This shows that the linear properties identified in Sec. III establish themselves very quickly. Considering now Figs. 5(b), 5(c), and 5(d) for the other three configurations we note that the pulses do not disperse, but interact in different ways. Figure 5(b) shows the coupled pulses from Configuration B weakly attract each other. In Figs. 5(c) and 5(d), corresponding to Configurations C and D, respectively, the pulses also attract, but more strongly, and seem to lead to the formation of a single pulse, which then separates into two distinct pulses. This process occurs multiple times. Although it appears to be periodic, particularly in Fig. 5(d), it cannot be since the process leads to the formation of radiation and so the pulse energies have to reduce over time. We note that in further propagation in Fig. 5(b) (not shown) there are always two distinct objects.

Figures 6(b), 6(c), and 6(d) are similar, except that the larger initial separation leads to a weaker interaction. This is most clearly seen in Figs. 6(c) and 6(d). Although the interaction in Fig. 6(b) is also weaker than in Fig. 5(b), the pulses now repel. This is consistent with our finding that the tails in Configuration B oscillate in time. Figures 5(b) and 6(b) show that this property is intrinsic to the dispersion and does not depend on the initial condition. The soliton tails are nonoscillating in Configurations C and D, and therefore the sign of interaction does not depend on the pulse separation.

VI. DISCUSSION AND CONCLUSIONS

We have successfully formulated an analytic framework to describe the behavior of bright pulselike solutions in the presence of even dispersion up to sixth-order dispersion. Taking methods previously employed for fourth-order dispersion,

we reduce the generalized nonlinear Schrödinger equation to Eq. (2), by enforcing that the solution is stationary. By neglecting the nonlinear term we study the low-amplitude tails of the pulses; we find four solution types and the corresponding boundaries between these solutions. Our results are confirmed numerically. Our methodology from Secs. II and III can be applied to any order. This means that we can use our framework to analytically predict the tail behavior of even dispersion solutions at arbitrary order, based on what we discern to be the dominant tail roots.

We identified two boundary types, μ_0 and μ_c, which separate exponential from oscillatory tail solutions. The transition over the μ_0 boundary from Region C to B, keeps the exponential decay rate (corresponding to the real part of the dominant root) constant. However, it introduces an oscillating component (corresponding to the imaginary part of the dominant root), the frequency of which increases as the dominant root becomes complex, while its amplitude remains approximately constant [24]. In contrast, the newly found transition across the μ_c boundary from Region D to B, keeps the frequency of the oscillating component of the tail approximately constant, but increases its amplitude as the purely real roots start to dominate.

As the order of dispersion increases, we expect to see an increasing variation in tail root configurations. However, the understanding of the dominant tail root that we have acquired allows us to predict the behavior as we consider these higher order dispersion systems. Apart from degenerate cases, we expect three types of transitions: the μ_0 and μ_c boundaries, as well as a boundary where the dominant behavior transitions between two complex quartets. This would lead to a change in the frequency of the tail oscillation, while the amplitude is approximately constant. Such a transition requires at least eighth-order dispersion and does not exist in the system we are considering here.

We found an exact analytic solution, in Sec. IV B, given by the cube of a hyperbolic secant, which corresponds to Configuration C. This family of solutions traces a curve through parameter space which remains in Region C. We have not been able to find any other exact analytic solutions in the parameter space. This exact solution is interesting in its own right, but also acts as a starting point for the numerical searches of solutions with different coefficients.

The solutions we found appear to be stable, persisting in propagation over 100 nonlinear lengths. Having established this we investigated the nature of soliton interactions. We found that in Configurations C and D, for which the tails exponentially decay, the sign of the interaction is independent of the mutual soliton distance. However, for Configuration B, for which the tails have additional oscillations, the sign of the interaction does depend on the mutual distance. We found that this is a property of the dispersion, independent of the initial condition which we kept as a constant Gaussian input. Although our analysis was qualitative and more sophisticated ODE-based models can be used to analyze these interactions [29], this is outside the scope of this work. Research involving soliton interactions to this point has largely been in the conventional soliton regime [29,30], or dealing with kink and antikink interactions [36,37]. The most recent studies involving interacting solitons including fourth-order dispersion, have studied the stability of multipulse systems, without rigorously examining the dynamics of these coupled soliton systems [38,39]. Thus, coupled soliton systems, in particular the unique behavior exhibited by solutions with oscillatory tails, have largely remained unexplored. Although our analysis has been qualitative, it suggests a rich area for future research.

ACKNOWLEDGMENTS

We acknowledge funding from Australian Research Project (ARC) Discovery Project No. DP180102234, and Asian Office of Aerospace R&D (AOARD) Grant No. FA2386-19-1-4067. The authors thank Dr. Antoine Runge for discussions and suggestions.

APPENDIX: FOUR-DIMENSIONAL PARAMETER SPACE—SPECIAL CASES

In this Appendix we consider two more special cases in addition to that in Sec. III A, namely $\beta_2 = 0$ (Sec. A 1) and μ is small and positive (Sec. A 2).

1. Nonzero β_4 and $\beta_2 = 0$

Setting $\beta_2 = 0$ we find the tail equation is

$$-\mu + \frac{\beta_4}{24}(\lambda^2)^2 + \frac{|\beta_6|}{720}(\lambda^2)^3 = 0, \tag{A1}$$

which, as in Sec. III A, we treat as a cubic equation in λ^2. For $\beta_4 > 0$ it may have one positive and two negative real roots (no pulselike solutions), or one positive root and a pair of complex roots (pulselike solutions). The boundary between these regions is given by

$$\mu_0 = \frac{50}{9}\frac{\beta_4^3}{|\beta_6|^2}, \tag{A2}$$

illustrated in Fig. 7 separating Regions A and B.

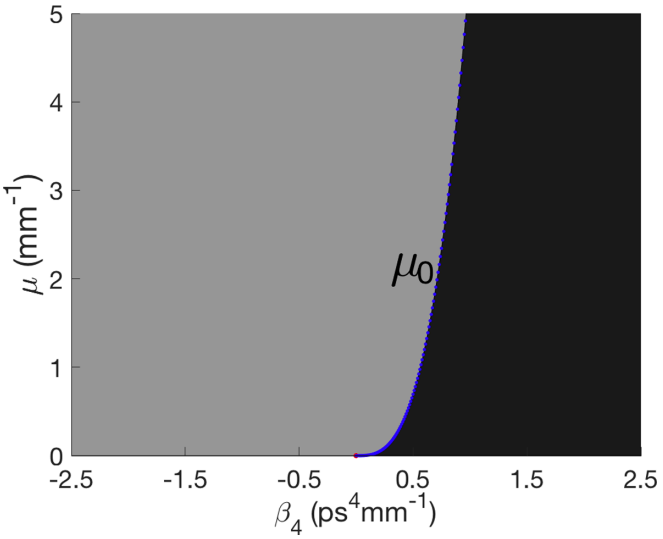

FIG. 7. Cross section through parameter space for $\beta_6 = -1$ ps^{6}mm^{-1} and $\beta_2 = 0$. The colors correspond to regions given in Table I (Regions A and B).

In contrast to the $\beta_4 = 0$ case (Sec. III A), roots for λ of the type $\pm a_r$ and $\pm a_r \pm i a_i$ are inconsistent with the requirement $\beta_2 = 0$, except for the trivial case $a_r = a_i = 0$, therefore there is no equivalent of the μ_c boundary. In fact it is straightforward to see that the complex roots always dominate for $\beta_2 = 0$. The corresponding parameter plane is shown in Fig. 7, with only the boundary μ_0.

2. Small, positive μ

We first consider $\mu = 0$, so that Eq. (3) reduces to

$$-\frac{\beta_2}{2}\lambda^2 + \frac{\beta_4}{24}\lambda^4 + \frac{|\beta_6|}{720}\lambda^6 = 0, \tag{A3}$$

which has the cubic roots,

$$\lambda^2 = 0, \text{ or } \lambda^2 = \frac{15\beta_4}{|\beta_6|}\left(-1 \pm \sqrt{1 + \frac{5}{8}\frac{\beta_2|\beta_6|}{\beta_4^2}}\right). \tag{A4}$$

When μ becomes small and positive the root at the origin shifts to the positive real axis when $\beta_2 < 0$ whereas it shifts to the negative real axis when $\beta_2 > 0$. From this we immediately see that there are no pulselike solutions when $\beta_2 > 0$. For $\beta_2 < 0$, the result depends on the sign of β_4 and the sign of the discriminant in Eq. (A4). When pulselike solutions do exist then the root near the origin dominates—therefore, all such solutions have exponential tails. With this information we construct Fig. 8.

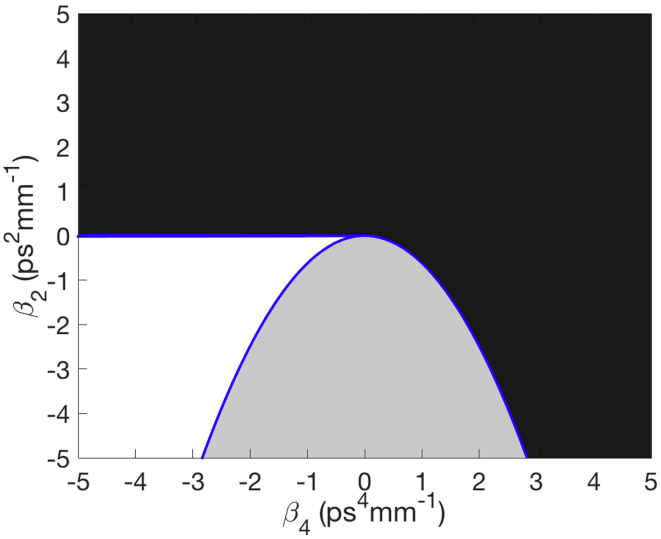

FIG. 8. Cross section through the parameter space for small, positive μ and $\beta_6 = -1$ ps^6 mm^{-1}. The colors correspond to regions given in Table I (Regions A, C, and D). The blue curve bounding Region D is given analytically by $\beta_2 = -8\beta_4^2/5\beta_6$.

The results in the specific cases discussed in Secs. III A, A 1, and A 2 give an indication of what may be expected in the general case. Although Fig. 8 does not show regions with oscillating tails we would expect these to become increasingly prominent as μ increases based on Figs. 2 and 7, particularly for small β_2 and $\beta_4 < 0$.

[1] A. Hasegawa and F. Tappert,Transmission of stationary nonlinear optical pulses in dispersive dielectric fibers. I. Anomalous dispersion, Appl. Phys. Lett. **23**, 142 (1973).

[2] A. Scott, F. Chu, and D. McLaughlin, The soliton: A new concept in applied science, Proc. IEEE **61**, 1443 (1973).

[3] F. Abdullaev, S. Darmanyan, P. Khabibullaev, and J. Engelbrecht, *Optical Solitons* (Springer, Berlin, 2014).

[4] N. N. Akhmediev and A. Ankiewicz, *Dissipative Solitons: From Optics to Biology and Medicine* (Springer, Berlin, 2011).

[5] G. P. Agrawal, *Nonlinear Fiber Optics* (Academic Press, Cambridge, 2013).

[6] S. K. Turitsyn, B. G. Bale, and M. P. Fedoruk, Dispersion-managed solitons in fibre systems and lasers, Phys. Rep. **521**, 135 (2012).

[7] F. M. Mitschke and L. F. Mollenauer, Ultrashort pulses from the soliton laser, Opt. Lett. **12**, 407 (1987).

[8] M. Nakazawa, Soliton transmission in telecommunication networks, IEEE Commun. Mag. **32**, 34 (1994).

[9] H. A. Haus and W. S. Wong, Solitons in optical communications, Rev. Mod. Phys. **68**, 423 (1996).

[10] P. Marin-Palomo, J. N. Kemal, M. Karpov, A. Kordts, J. Pfeifle, M. H. P. Pfeiffer, P. Trocha, S. Wolf, V. Brasch, M. H. Anderson, R. Rosenberger, K. Vijayan, W. Freude, T. J. Kippenberg, and C. Koos, Microresonator-based solitons for massively parallel coherent optical communications, Nature (London) **546**, 274 (2017).

[11] P. Rohrmann, A. Hause, and F. Mitschke, Solitons beyond binary: Possibility of fibre-optic transmission of two bits per clock period, Sci. Rep. **2**, 00866 (2012).

[12] J. M. Dudley, G. Genty, and S. Coen, Supercontinuum generation in photonic crystal fiber, Rev. Mod. Phys. **78**, 1135 (2006).

[13] A. V. Husakou and J. Herrmann, Supercontinuum Generation of Higher-Order Solitons by Fission in Photonic Crystal Fibers, Phys. Rev. Lett. **87**, 203901 (2001).

[14] K. Sakamaki, M. Nakao, M. Naganuma, and M. Izutsu, Soliton induced supercontinuum generation in photonic crystal fiber, IEEE J. Sel. Top. Quantum Electr. **10**, 876 (2004).

[15] M. Karlsson and A. Höök, Soliton-like pulses governed by fourth-order dispersion in optical fibers, Opt. Commun. **104**, 303 (1994).

[16] N. Akhmediev, A. Buryak, and M. Karlsson, Radiationless optical solitons with oscillating tails, Opt. Commun. **110**, 540 (1994).

[17] M. Piché, J.-F. Cormier, and X. Zhu, Bright optical soliton in the presence of fourth-order dispersion, Opt. Lett. **21**, 845 (1996).

[18] Y. Kodama, M. Romagnoli, M. Midrio, and S. Wabnitz, Role of third-order dispersion on soliton instabilities and interactions in optical fibers, Opt. Lett. **19**, 165 (1994).

[19] T. I. Lakoba and G. P. Agrawal, Effects of third-order dispersion on dispersion-managed solitons, J. Opt. Soc. Am. B **16**, 1332 (1999).

[20] S. Roy, S. K. Bhadra, and G. P. Agrawal, Dispersive waves emitted by solitons perturbed by third-order dispersion inside optical fibers, Phys. Rev. A **79**, 023824 (2009).

[21] B. A. Malomed, D. J. Frantzeskakis, H. E. Nistazakis, A. Tsigopoulos, and K. Hizanidis, Dissipative solitons under the action of the third-order dispersion, Phys. Rev. E **60**, 3324 (1999).

[22] K. C. Chan and H. F. Liu, Effect of third-order dispersion on soliton-effect pulse compression, Opt. Lett. **19**, 49 (1994).

[23] K. K. K. Tam, T. J. Alexander, A. Blanco-Redondo, and C. M. de Sterke, Stationary and dynamical properties of pure-quartic solitons, Opt. Lett. **44**, 3306 (2019).

[24] K. K. K. Tam, T. J. Alexander, A. Blanco-Redondo, and C. M. de Sterke, Generalized dispersion Kerr solitons, Phys. Rev. A **101**, 043822 (2020).

[25] A. Blanco-Redondo, C. M. de Sterke, J. E. Sipe, T. F. Krauss, B. J. Eggleton, and C. Husko, Pure-quartic solitons, Nat. Commun. **7**, 10427 (2016).

[26] A. F. J. Runge, D. D. Hudson, K. K. K. Tam, C. M. de Sterke, and A. Blanco-Redondo, The pure-quartic soliton laser, Nat. Photon. **14**, 492 (2020).

[27] A. F. J. Runge, Y. L. Qiang, T. J. Alexander, M. Z. Rafat, D. D. Hudson, A. Blanco-Redondo, and C. M. de Sterke, Infinite hierarchy of solitons: Interaction of Kerr nonlinearity with even orders of dispersion, Phys. Rev. Research **3**, 013166 (2021).

[28] J. P. Lourdesamy, A. F. J. Runge, T. J. Alexander, D. D. Hudson, A. Blanco-Redondo, and C. M. de Sterke, Spectrally periodic pulses for enhancement of optical nonlinear effects, Nat. Phys. **18**, 59 (2021).

[29] N. Manton, An effective Lagrangian for solitons, Nucl. Phys. B **150**, 397 (1979).

[30] H. Baron and W. Zakrzewski, Collective coordinate approximation to the scattering of solitons in modified NLS and sine-Gordon models, J. High Energy Phys. 06 (2016) 185.

[31] R. S. Irving, *Integers, Polynomials, and Rings: A Course in Algebra* (Springer, Berlin, 2004).

[32] J. Yang, Newton-conjugate-gradient methods for solitary wave computations, J. Comput. Phys. **228**, 7007 (2009).

[33] V. Zakharov and A. B. Shabat, Exact theory of two-dimensional self-focusing and one-dimensional self-modulation of waves in nonlinear media, Sov. J. Exp. Theor. Phys. **34**, 62 (1972).

[34] M. J. Ablowitz and H. Segur, *Solitons and the Inverse Scattering Transform* (Society for Industrial and Applied Mechanics, Philadelphia, 1981).

[35] A. Höök and M. Karlsson, Ultrashort solitons at the minimum-dispersion wavelength: effects of fourth-order dispersion, Opt. Lett. **18**, 1388 (1993).

[36] N. S. Manton, Forces between kinks and antikinks with long-range tails, J. Phys. A: Math. Theor. **52**, 065401 (2019).

[37] N. S. Manton and H. Merabet, ϕ^4 kinks-gradient flow and dynamics, Nonlinearity **10**, 3 (1997).

[38] R. I. Bandara, A. Giraldo, N. G. R. Broderick, and B. Krauskopf, Infinitely many multipulse solitons of different symmetry types in the nonlinear Schrödinger equation with quartic dispersion, Phys. Rev. A **103**, 063514 (2021).

[39] R. Parker and A. Aceves, Multi-pulse solitary waves in a fourth-order nonlinear Schrödinger equation, Physica D **422**, 132890 (2021).